Atmospheric Environment 43 (2009) 5894–5907

Contents lists available at ScienceDirect

Atmospheric Environment

journal homepage: www.elsevier.com/locate/atmosenv

Contribution of transboundary air pollution to ionic concentrations in fog in the Kinki Region of Japan

Hikari Shimadera*,[1], Akira Kondo, Akikazu Kaga, Kundan Lal Shrestha, Yoshio Inoue

Graduate School of Engineering, Osaka University, Japan

ARTICLE INFO

Article history:
Received 9 June 2009
Received in revised form
21 August 2009
Accepted 21 August 2009

Keywords:
Fog
Long-range transport
East Asia
CMAQ
MM5

ABSTRACT

To estimate the contribution of transboundary transported air pollutants from other Asian countries to Japan in ionic concentrations in fog water in March 2005, the Community Multiscale Air Quality (CMAQ) modeling system was utilized with meteorological fields produced by the 5th generation Mesoscale Model (MM5). For meteorological predictions, the model well reproduced the surface meteorological variables, particularly temperature and humidity, and generally captured fog occurrence. For chemical predictions, most of the model-predicted monthly mean concentrations were approximately within a factor of 2 of the observations, indicating that the model well simulated the long-range atmospheric transport from the Asian Continent to Japan. For SO_4^{2-}, NO_3^- and NH_4^+, the contribution rates of the transboundary air pollution in the Kinki Region of Japan ranged from 69 to 82% for aerosols, from 47 to 87% for ionic concentrations in rain, and from 55 to 79% for ionic concentrations in fog. The study found that the transboundary air pollution also affected ionic concentrations in fog as well as aerosol concentrations and ionic concentrations in rain.

1. Introduction

Substantial economic growth and increased energy consumption have resulted in increased anthropogenic emissions of air pollutants such as SO_2, NO_x, CO, non-methane hydrocarbons (NMHCs) and particulate matter (PM) have increased in East Asia, particularly in China. Richter et al. (2005) reported that tropospheric NO_2 in satellite measurements over the industrial area of China increased approximately 50% during 1996–2004 with the accelerating annual growth rate, indicating a significant increase in NOx emissions over the period. Ohara et al. (2007) estimated that total energy consumption more than doubled and anthropogenic emissions increased by 119% for SO_2, 176% for NO_x, 64% for CO, 108% for NM volatile organic compounds (NMVOCs) in Asia during 1980–2003. In addition, Zhang et al. (2009) estimated that anthropogenic emissions in China increased by 36% for SO_2, 55% for NO_x, 18% for CO, 29% for VOCs and 13% for PM_{10} during 2001–2006.

As air pollutant emissions have increased, long-range transport and fate of air pollutants have become a field of scientific interests in East Asia. Zhang et al. (2006) investigated the transport and transformation processes of O_3 and its closely related precursors such as OH, HO_2 and NO_x in East Asia. Lin et al. (2008) quantified the region-to-region source–receptor relationships for total sulfur and total reactive nitrogen deposition in East Asia. Chemical transport models (CTMs), such as the U.S. Environmental Protection Agency's (EPA) Models-3 Community Multiscale Air Quality (CMAQ) modeling system (Byun and Ching, 1999; Byun and Schere, 2006), have become critical tools for the studies of long-range atmospheric transport. Various regional modeling groups have applied CTMs to East Asia in the model intercomparison study for Asia (MICS-Asia), which have been carried out during 1998–2002 as Phase I (Carmichael et al., 2002) and after 2003 as Phase II (Carmichael et al., 2008). In MICS-Asia Phase I, 8 long-range transport models were involved for the study of sulfur deposition. In MICS-Asia Phase II, 9 different regional modeling groups simulated chemistry and transport of O_3, secondary aerosols, acid deposition, and associated precursors. Furthermore, the effects of long-range pollutant transport have been intensively studied in Japan (e.g., Ichikawa et al., 1998; Tamamura et al., 2007), which tends to be downwind of the Asian Continent and to be strongly affected by the continental outflow.

The studies of long-range atmospheric transport related to O_3 and its precursors, aerosols, dry and wet depositions have been widely conducted using CTMs, but those related to fog chemistry have not. Fog affects forest ecosystems in mountainous and coastal areas, in which fog occurs more frequently than in other areas. Fog water deposition through the interception of fog droplets by

* Corresponding author. Division of Sustainable Energy and Environmental Engineering, Graduate School of Engineering, Osaka University, 2-1 Yamadaoka, Suita, Osaka 565-0871, Japan. Tel./fax: +81 06 0879 7670.
E-mail address: shimadera@ea.see.eng.osaka-u.ac.jp (H. Shimadera).
[1] Research Fellow of the Japan Society for the Promotion of Science (DC).

1352-2310/$ – see front matter © 2009 Elsevier Ltd. All rights reserved.
doi:10.1016/j.atmosenv.2009.08.022

vegetation can be an important part of the hydrologic budget of forests (Vong et al., 1991; Dawson, 1998; Eugster et al., 2006). Ionic concentrations in fog water are much higher than those in rain water (Igawa et al., 1998; Neal et al., 2003; Aikawa et al., 2006). Consequently, fog can contribute significantly to the deposition of ionic compounds in mountainous forest areas (Kobayashi et al., 2001; Baumgardner et al., 2003). The effects of fog may be more pronounced in Japan than in other countries because approximately two-thirds of the land area is covered by forests, most of which are located in mountainous regions. The study of fog on a spatial scale requires numerical simulations because few fog monitoring sites exist and fog is highly variable according to regions. In the field of fog simulations, one-dimensional models have been applied to investigations of fog physics (e.g., Zdunkowski and Nielsen, 1969; Brown, 1980; Musson-Genon, 1987). More recently, mesoscale models, such as the 5th generation Penn State University (PSU)/National Center for Atmospheric Research (NCAR) Mesoscale Model (MM5) (Grell et al., 1994) and the Regional Atmospheric Modeling System (RAMS) (Pielke et al., 1992), have been employed for regional forecasting of particular fog events (e.g., Ballard et al., 1991; Pagowski et al., 2004; Fu et al., 2006). The previous study applied MM5 version 3.7 to fog simulation for months over the Kinki Region of Japan, and showed that the model reproduced general trends in fog occurrence (Shimadera et al., 2008).

The present study utilized CMAQ modeling system version 4.7 with meteorological fields produced by MM5 version 3.7 to estimate contribution rates of the transboundary transported air pollutants from other Asian countries to the Kinki Region of Japan for concentrations of SO_4^{2-}, NO_3^-, NH_4^+ in fog water, in addition to those for concentrations of gaseous SO_2, NO_x, HNO_3, NH_3, suspended PM (SPM), aerosol SO_4^{2-}, NO_3^-, NH_4^+, and SO_4^{2-}, NO_3^-, NH_4^+ in rain water.

2. Methods

2.1. Model setup

The models used in the present study include MM5 version 3.7 and CMAQ version 4.7. MM5 is a three-dimensional, nonhydrostatic, terrain-following sigma-pressure coordinate model with a multiple-nest capability, several physics options, and a four-dimensional data assimilation capability. The model is widely used to drive air quality models (e.g., Sokhi et al., 2006; Tesche et al., 2006). CMAQ is a three-dimensional Eulerian air quality modeling system that simulates the transport, transformation, and deposition of various air pollutants and their precursors across spatial scales ranging from local to hemispheric. For the current study, CMAQ was modified to output ionic concentrations in cloud water at the first (lowest) layer, i.e. fog water. The following equation for horizontal visibility (x_{vis}) obtained from Stoelinga and Warner (1999) was utilized to judge whether fog occurred or not.

$$x_{vis} = -1000 \times \frac{\ln(0.02)}{144.7\mathrm{LWC}^{0.88}}, \quad (1)$$

where LWC is liquid water content of fog. It was considered that fog occurred when $x_{vis} < 1000$ m, i.e. LWC > 0.017 g m^{-3} according to Eq. (1).

Fig. 1 shows modeling domains for CMAQ prediction. The study region is centered at (122.5°E, 32.5°N) on the Lambert conformal conic projection map of East Asia. The horizontal domains consist of 4 domains from domain 1 (D1) covering a wide area of East Asia to domain 4 (D4) covering most of the Kinki Region of Japan. The horizontal resolutions and the number of grid cells in the domains are 54, 18, 6 and 2 km, and 105×81, 72×72, 99×99 and 126×126 for D1, domain 2 (D2), domain 3 (D3) and D4, respectively. Finer grid resolution enables the MM5/CMAQ modeling system to better reproduce complex topographic structures in Japan, and therefore to better capture fog occurrence because fog is highly variable according to regions and fog frequency generally increases with altitude. Thus this study uses the horizontal resolution of 2 km in D4 while many other studies of long-range atmospheric transport over East Asia with CTMs use horizontal resolutions of coarser than 20 km (e.g., Zhang et al., 2006; Carmichael et al., 2008; Lin et al., 2008). The vertical layers consist of 24 sigma-pressure coordinated layers from the surface to 100 hPa with approximately 15 m as the middle height of the first layer.

For meteorological prediction, MM5 was configured with the scheme of Grell et al. (1994) for the cumulus parameterization, the medium range forecast scheme (Hong and Pan, 1996) for planetary

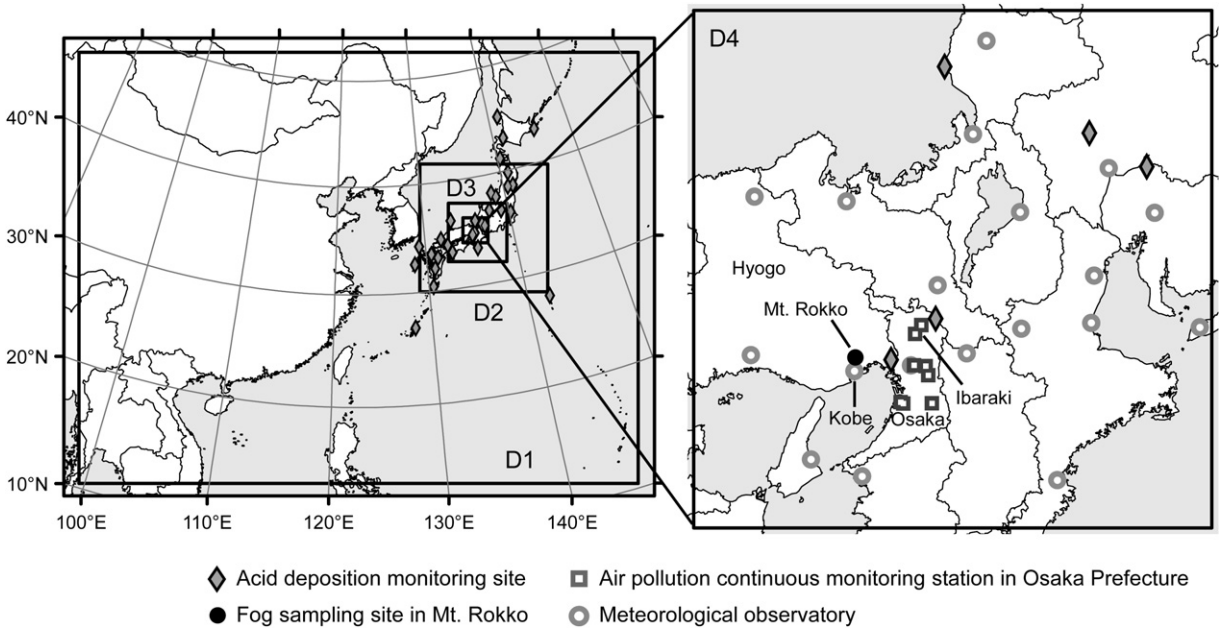

Fig. 1. Modeling domains and locations of observation sites.

boundary layer parameterization, the schemes of Dudhia (1989) for the cloud microphysics and the radiation simulations, and the Noah land surface model (Chen and Dudhia, 2001) for the land surface interactions. The input data for MM5 include the National Centers for Environmental Prediction final analysis (NCEP FNL) data, and the grid point value derived from the mesoscale model (GPV MSM) data by JMA. The NCEP FNL data are global analysis data with a spatial resolution of $1^\circ \times 1^\circ$ and a temporal resolution of 6 h. The GPV MSM data are available for the Japan region and have a high spatial resolution of 0.125° (for longitude) $\times$ 0.1° (for latitude) and a temporal resolution of 3 h. Initial and boundary conditions for MM5 were obtained from the NCEP FNL for D1, and the GPV MSM for D2. Therefore, there is no interaction between D1 and D2 in the meteorological prediction. Boundary conditions for D3 and D4 were updated every hour from the MM5 output files for D2 and D3, respectively. The MM5 hourly output files were processed using the Meteorology–Chemistry Interface Processor (MCIP) version 3.4 for CMAQ.

For chemical prediction, CMAQ was configured with the Statewide Air Pollution Research Center version 99 (SAPRC99) (Carter, 2000) mechanism for the gas-phase chemistry, the 5th generation CMAQ aerosol module (AERO5) for the aerosol processes, and the cloud and aqueous phase chemistry option. Initial and boundary conditions for D1 were obtained from the CMAQ default concentration profiles. Boundary conditions for D2, D3 and D4 were updated every hour from the CMAQ output files for D1, D2 and D3, respectively.

The MM5/CMAQ modeling system was run for March 2005, in which fog sampling data at Mt. Rokko were available for the model evaluations, with an initial spin-up period of 5 days (24–28 February 2005). The Japan region tends to be more affected by the Asian continental outflows in winter and spring (Seto et al., 2002), making March a suitable month for the investigation of long-range atmospheric transport.

2.2. Emission data

Emission data applied in this study include anthropogenic, biogenic VOCs (BVOCs), biomass burning and volcanic SO_2 emissions. Anthropogenic and BVOCs emissions for the Japan region were derived from EAGrid2000-Japan (Kannari et al., 2007). EAGrid2000-Japan is an emissions inventory for Japan with a high spatial resolution of 45″ (for longitude) $\times$ 30″ (for latitude) and a temporal resolution of 1 h for weekdays and holidays in every month of 2000. In Japan, air pollution in roadside areas has been improving since the Law concerning Special Measures for Total Emission Reduction of Nitrogen Oxides and Particulate Matter from Automobiles in Specified Areas (Automobile NOx/PM Law) was enacted in 2001. To reflect the situation, vehicles' exhaust emissions in EAGrid2000-Japan were cut according to decreasing rates of air pollutant concentrations observed at the roadside air pollution monitoring stations in Hyogo Prefecture. The decreasing rates during 2000–2005 were 43% for SO_2, 20% for NO_x, 28% for CO, 22% for NMHCs, 16% for SPM.

For the other Asian countries, anthropogenic emissions of SO_2, NO_x, CO, VOCs and PM were obtained from an emissions inventory for Asia in the year 2006 with a $0.5^\circ \times 0.5^\circ$ spatial resolution developed to support the Intercontinental Chemical Transport Experiment-Phase B (INTEX-B) (Zhang et al., 2009). Emissions of NH_3 were derived from predicted values for the year 2005 in regional emission inventory in Asia (REAS) with a $0.5^\circ \times 0.5^\circ$ spatial resolution (Ohara et al., 2007). BVOCs and biomass burning emissions were derived from Murano (2006) and Streets et al. (2003), with $0.5^\circ \times 0.5^\circ$ and $1^\circ \times 1^\circ$ spatial resolutions, respectively.

The volcanic SO_2 emission fluxes were obtained from Andres and Kasgnoc (1998) for volcanoes erupting SO_2 continuously, and observation data by JMA in March 2005 for Miyakejima located to the south of Tokyo. In addition, sea salt emissions were calculated within the AERO5 module as a function of wind speed and relative humidity, following the parameterizations of Gong (2003) and Zhang et al. (2005), respectively.

To estimate the contribution of the transboundary air pollution, model simulations were conducted in two emission cases. One was a baseline case with the total emissions described above (EB), and the other was a case with emissions only from the Japan region (EJ). Fig. 2 shows spatial distributions of SO_2, NO_x and NH_3 emission rates in EB, EJ and D4. The total emission rates of SO_2 are 19 016 mol s^{-1} in EB and 1714 mol s^{-1}, 75% of which is accounted for by the volcanic emissions (1279 mol s^{-1}), in EJ.

2.3. Observation data

The observation data used for model evaluations were obtained from fog sampling on Mt. Rokko conducted by the Hyogo Prefectural Government, meteorological observation at 19 observatories in D4 conducted by the Japan Meteorological Agency (JMA), air pollution continuous monitoring and SPM sampling at the 8 monitoring stations conducted by the Osaka Prefectural Government, and acid deposition monitoring at 30 sites by the Ministry of the Environment (MOE) of Japan. The locations of observation sites are shown in Fig. 1. The fog sampling was performed by using an active string-fog collector for research on acid fog at (135°13′45″ E, 34°45′24″N) with an altitude of 800 m on Mt. Rokko. The details of the sampling method and composition of the collector are described in Aikawa et al. (2005). The air pollution monitoring in Osaka Prefecture employs automatic monitoring systems for hourly measurements of air pollutants such as NO_x, SO_2, CO, O_3 and SPM, and Andersen samplers for measurements of biweekly integrated values of PM compositions. The acid deposition monitoring by MOE employs wet-only samplers for measurements of daily (weekly, biweekly or monthly at some sites) integrated values of wet depositions, and automatic monitoring systems for hourly measurements of NO_x, SO_2, O_3 and PM at some sites, and filter packs for measurements of weekly or biweekly integrated values of SO_2, HCl, HNO_3, NH_3 and PM compositions at the Acid Deposition Monitoring Network in East Asia (EANET) stations.

3. Meteorological predictions

Fig. 3 shows hourly time series of observed and model-predicted temperature, humidity, precipitation and wind speed at the Kobe meteorological observatory, which is located at approximately 10 km south of the fog sampling site in Mt. Rokko (Fig. 1). The model predictions for temperature and humidity in D4 were in fairly good agreement with the observations throughout March 2005. The humidity levels rose significantly on some days. The model approximately captured the precipitation periods and the amount of precipitation during each event. For wind speed, wind U- and V-components, the discrepancies between the observations and predictions were relatively large compared to those for temperature and humidity, but the model predictions generally followed the pattern of observations. Fig. 4 shows hourly time series of observed and model-predicted LWC at the Mt. Rokko fog sampling site. Occurrences of fog on Mt. Rokko were associated with the high humidity periods at the Kobe observatory (Fig. 3b), and were well captured by the model. However, the model tended to overestimate LWC, with the observed and model-predicted mean LWCs being 0.14 g m^{-3} and 0.37 g m^{-3}, respectively.

The model performance for meteorological predictions was evaluated using the statistical measures for benchmarks reported by Emery et al. (2001). The statistical measures include the mean

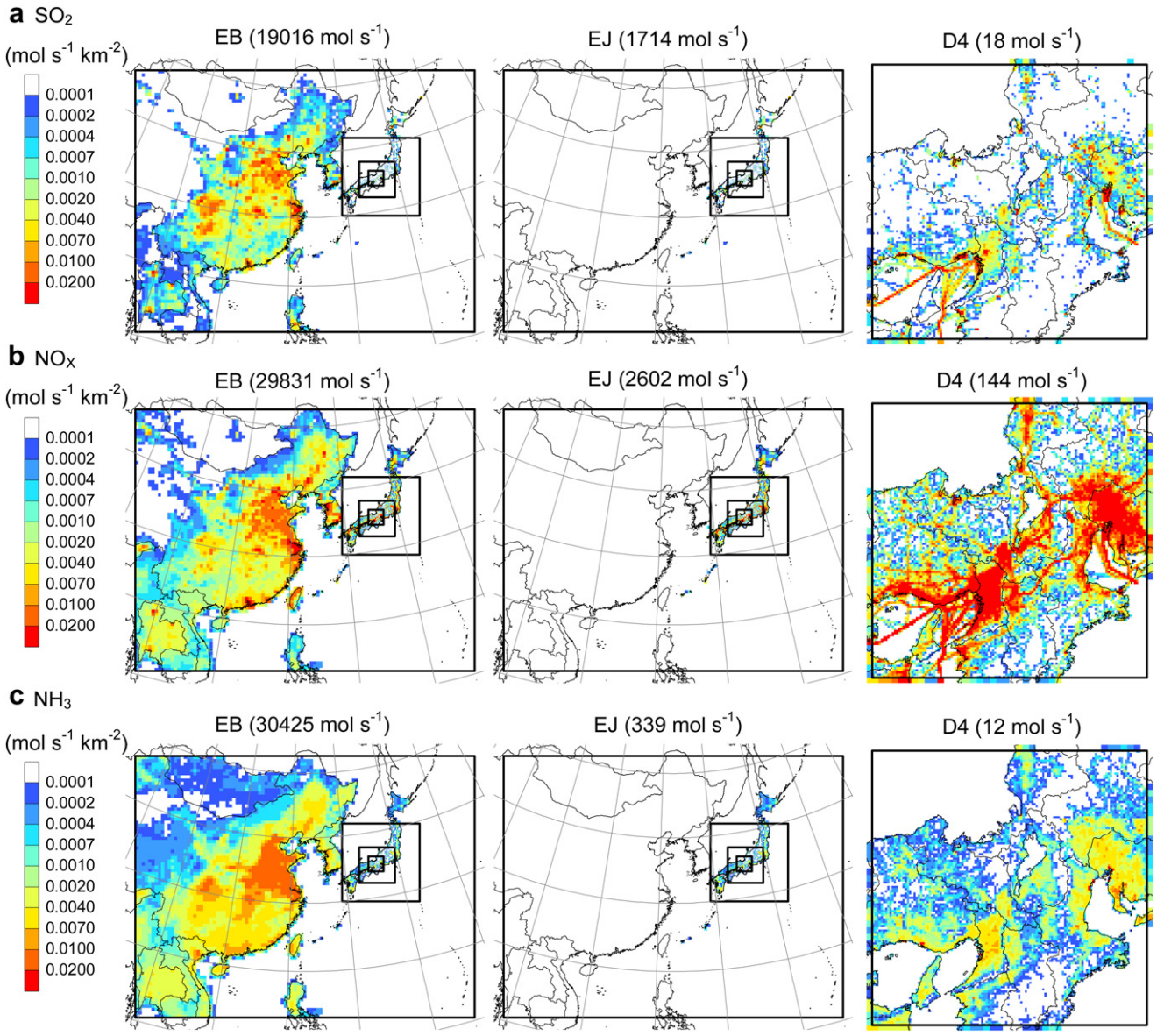

Fig. 2. Spatial distributions of SO_2, NO_x and NH_3 emission rates in EB, EJ and D4. Values in brackets are total emission rates.

bias error (MBE), the mean absolute error (MAE), the root mean square error (RMSE) and the index of agreement (IA). The statistical measures are defined as

$$\mathrm{MBE} = \overline{M} - \overline{O}, \tag{2}$$

$$\mathrm{MAE} = \frac{1}{N}\sum_{i=1}^{N}|M_i - O_i|, \tag{3}$$

$$\mathrm{RMSE} = \left[\frac{1}{N}\sum_{i=1}^{N}(M_i - O_i)^2\right]^{1/2}, \tag{4}$$

$$\mathrm{IA} = 1 - \frac{\sum_{i=1}^{N}(M_i - O_i)^2}{\sum_{i=1}^{N}(|M_i - \overline{O}| + |O_i - \overline{O}|)^2}, \tag{5}$$

where $\overline{M}$ and $\overline{O}$ are mean model-predicted and observed values, M_i and O_i are model-predicted and observed values, and N is the number of samples, respectively. The model performance for hourly meteorological predictions is shown in Table 1 with monthly values, the Pearson's correlation coefficient (R), and the statistical measures described above for the 19 meteorological observatories including the Kobe observatory in D4 and the Kobe observatory. The model performance for D1 was worst among the 4 domains, which could be attributed to its coarse horizontal resolution and more likely to the difference in the analysis data used for the initial and boundary conditions (NCEP FNL for D1 and GPV MSM for the other domains). The accuracy of the model predictions at the Kobe observatory was similar to or slightly better than that at the other meteorological observatories. For temperature, the model met the benchmarks for all of MBE, MAE and IA in D3 and D4, and the benchmarks for MAE and IA in D2. For humidity, the model met all the benchmarks in all the domains. The model performance for wind speed was inferior to that for temperature and humidity, but the model met the benchmark for IA in D2, D3 and D4. Results in some other studies with

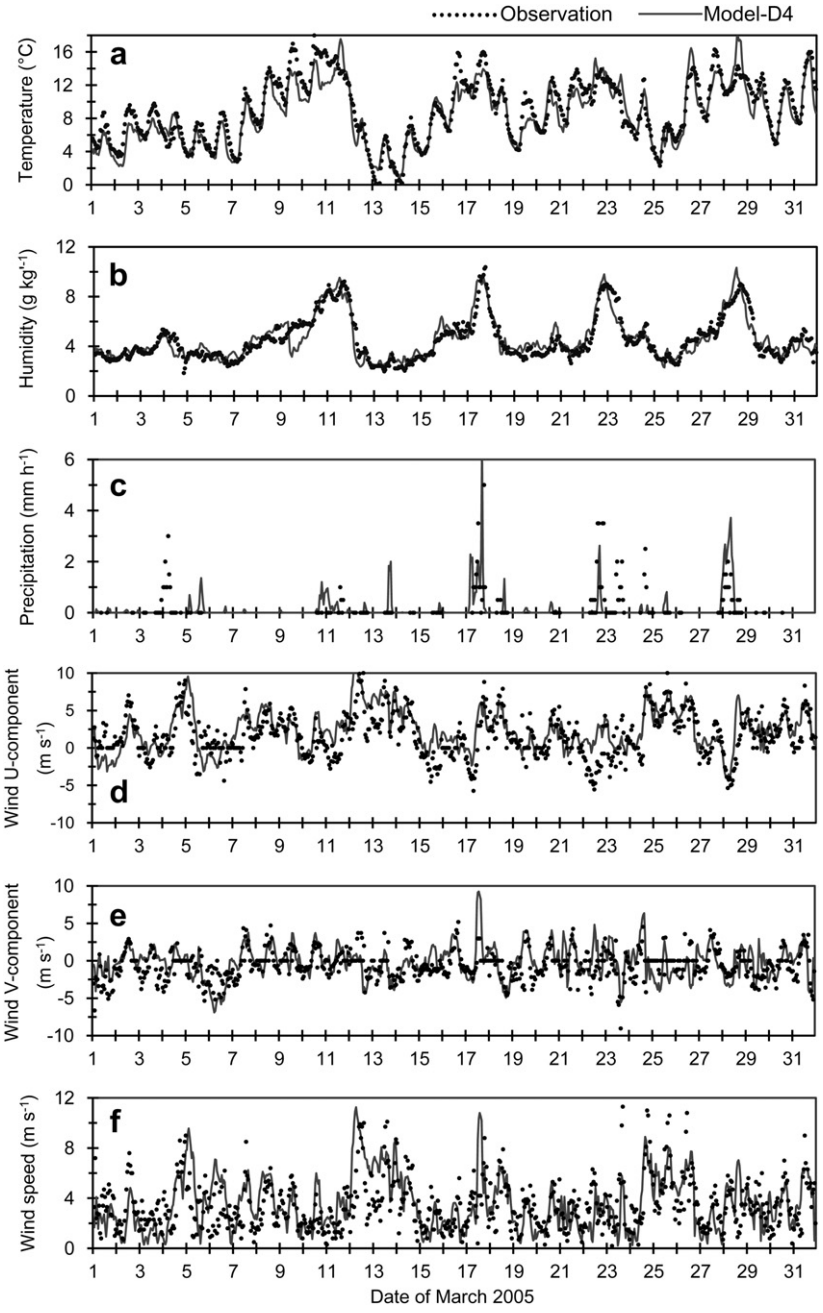

Fig. 3. Hourly time series of observed and model-predicted temperature, humidity, precipitation and wind speeds at the Kobe meteorological observatory in March 2005.

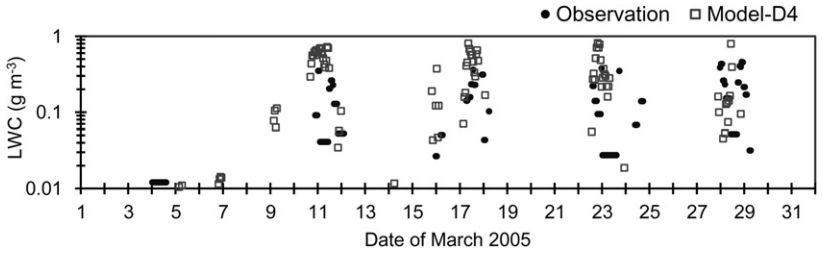

Fig. 4. Hourly time series of observed and model-predicted LWC at the Mt. Rokko fog sampling site in March 2005.

Table 1
Statistical measures for hourly meteorological predictions at the 19 meteorological observatories in D4 and the Kobe observatory in March 2005.

		The 19 observatories in D4				Kobe	Benchmarks
		D1	D2	D3	D4	D4	
Temperature	Mean observation (°C)	7.6	7.6	7.6	7.6	9.0	
	Mean prediction (°C)	5.0	6.7	7.2	8.0	8.4	
	R	0.73	0.85	0.87	0.89	0.92	
	MBE (°C)	−2.6	−1.0	−0.4	0.4	−0.6	≤±0.5
	MAE (°C)	3.2	2.0	1.8	1.6	1.2	≤2
	IA	0.78	0.90	0.93	0.94	0.95	≥0.8
Humidity	Mean observation (g kg^{-1})	4.3	4.3	4.3	4.3	4.5	
	Mean prediction (g kg^{-1})	4.4	4.5	4.5	4.5	4.6	
	R	0.81	0.88	0.89	0.89	0.91	
	MBE (g kg^{-1})	0.0	0.2	0.2	0.2	0.1	≤±1
	MAE (g kg^{-1})	0.7	0.6	0.6	0.6	0.6	≤2
	IA	0.89	0.94	0.94	0.94	0.95	≥0.6
Wind speed	Mean observation (m s^{-1})	3.0	3.0	3.0	3.0	3.4	
	Mean prediction (m s^{-1})	5.0	4.8	4.4	4.0	3.6	
	R	0.29	0.45	0.54	0.54	0.56	
	MBE (m s^{-1})	2.0	1.8	1.4	1.1	0.1	≤±0.5
	RMSE (m s^{-1})	3.3	3.1	2.7	2.5	2.0	≤2
	IA	0.51	0.60	0.67	0.69	0.75	≥0.6
Wind U-component	Mean observation (m s^{-1})	1.2	1.2	1.2	1.2	1.7	
	Mean prediction (m s^{-1})	2.7	2.8	2.3	2.0	2.3	
	R	0.37	0.50	0.55	0.56	0.68	
	MBE (m s^{-1})	1.5	1.6	1.1	0.9	0.6	
	RMSE (m s^{-1})	2.8	2.7	2.3	2.1	1.8	
	IA	0.58	0.64	0.70	0.72	0.81	
Wind V-component	Mean observation (m s^{-1})	−0.7	−0.7	−0.7	−0.7	−0.6	
	Mean prediction (m s^{-1})	−0.7	−0.5	−0.5	−0.5	−0.2	
	R	0.28	0.55	0.59	0.59	0.49	
	MBE (m s^{-1})	0.0	0.2	0.2	0.2	0.4	
	RMSE (m s^{-1})	3.8	2.8	2.6	2.5	2.1	
	IA	0.53	0.72	0.75	0.75	0.70	
Precipitation	Monthly observation (mm)	108	108	108	108	82	
	Monthly prediction (mm)	184	130	127	116	96	

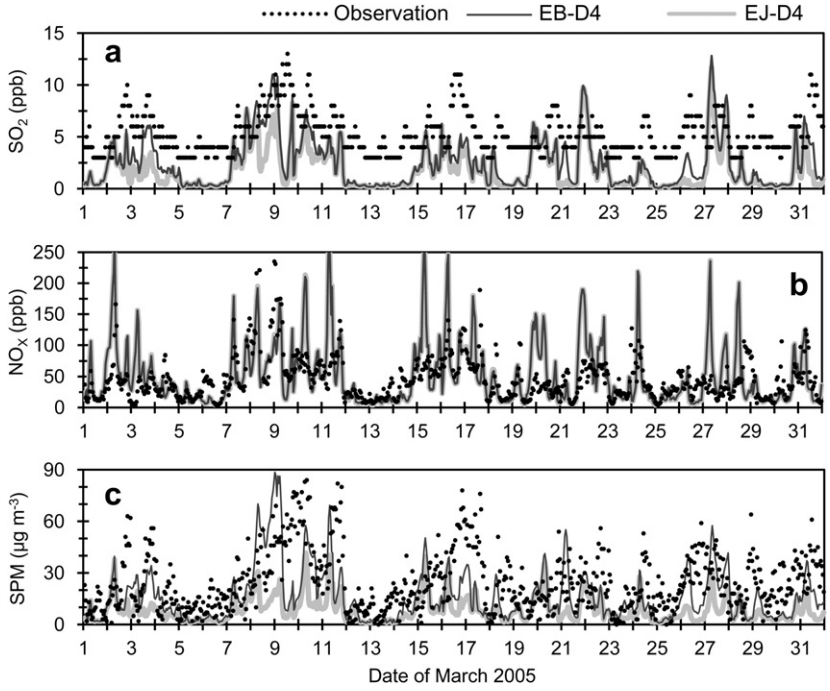

Fig. 5. Hourly time series of observed and model-predicted SO_2, NO_x and SPM concentrations at the Ibaraki monitoring station in March 2005.

Table 2
Statistical measures for hourly SO_2, NO_x and SPM predictions at the 8 monitoring stations in Osaka Prefecture and the Ibaraki monitoring station in March 2005.

		The 8 stations		Ibaraki	
		EB-D4	EJ-D4	EB-D4	EJ-D4
SO_2	Mean observation (ppb)	5.8	5.8	5.3	5.3
	Mean prediction (ppb)	3.5	3.0	2.4	1.9
	R	0.50	0.41	0.50	0.35
	MBE (ppb)	−2.3	−2.8	−2.8	−3.3
	MAE (ppb)	3.1	3.4	3.2	3.6
	IA	0.59	0.52	0.54	0.46
NO_x	Mean observation (ppb)	50.5	50.5	45.7	45.7
	Mean prediction (ppb)	47.4	47.6	51.3	51.6
	R	0.46	0.46	0.56	0.56
	MBE (ppb)	−3.2	−2.9	5.7	5.9
	MAE (ppb)	29.0	29.0	27.2	27.4
	IA	0.65	0.66	0.71	0.71
SPM	Mean observation (μg m^{-3})	29.5	29.5	24.6	24.6
	Mean prediction (μg m^{-3})	17.0	9.1	16.1	8.6
	R	0.42	0.37	0.44	0.33
	MBE (μg m^{-3})	−12.6	−20.4	−8.6	−16.0
	MAE (μg m^{-3})	17.0	21.2	14.8	17.7
	IA	0.59	0.48	0.64	0.50

MM5 also indicated such different tendencies between temperature and wind (e.g., Lee et al., 2007; Wu et al., 2008). For precipitation, the model generally reproduced but slightly overestimated the monthly amount in D2, D3 and D4. Overall, the model well reproduced the meteorological variables, particularly temperature and humidity, at the meteorological observatories in March 2005.

4. Chemical predictions

4.1. Temporal variations of SO_2, NO_x and SPM in Osaka Prefecture

Fig. 5 shows hourly time series of observed and model-predicted SO_2, NO_x and SPM concentrations at the Ibaraki monitoring station (Fig. 1), which was chosen as an example from the 8 monitoring stations in Osaka Prefecture. The model predictions for NO_x often failed to reproduce the daily peak concentrations, but generally followed the pattern of observations. The results of NO_x predictions for EB and EJ were quite consistent. For SO_2 and SPM, the model tended to underestimate the concentration levels, but generally reproduced the periods of high concentration. The concentrations in EB were often much higher than those in EJ, indicating that large amounts of SO_2 and SPM were transported from the Asian Continent to Japan in March 2005.

The model performance for hourly SO_2, NO_x and SPM predictions is shown in Table 2 with the statistical measures for the 8 monitoring stations including the Ibaraki monitoring station in Osaka Prefecture and the Ibaraki monitoring station. The accuracy of the model predictions at the Ibaraki monitoring station was similar to that at the other monitoring stations. The model performances for NO_x predictions in EB and EJ were almost consistent as NO_x tends to be a local pollutant. For SO_2 and SPM, the model showed better performance in EB than in EJ in terms of all the statistical measures, indicating that the model well simulated the long-range transport of air pollutants. The results imply that although the model resulted in some inaccurate surface wind predictions at the meteorological observatories, the model successfully simulated the synoptic wind fields controlling the atmospheric transport over East Asia.

4.2. Temporal variations of ionic concentrations in fog on Mt. Rokko

Fig. 6 shows hourly time series of observed and model-predicted SO_4^{2-}, NO_3^- and NH_4^+ concentrations in fog water at the Mt. Rokko fog sampling site. For all the three ions, the model tended to underestimate the concentrations in fog water. The concentrations in EB were consistently higher than those in EJ. As a result, monthly mean ionic concentrations in fog water for the observations, EB-D4 and EJ-D4 were 198, 76 and 27 μmol L^{-1} for SO_4^{2-}, 264, 127 and 48 μmol L^{-1} for NO_3^-, and 349, 123 and 25 μmol L^{-1} for NH_4^+, respectively. Most of the underestimations of ionic concentrations by the model were probably attributed to the overestimations of LWC (Fig. 4). The concentrations in EB were particularly higher on 10–11 March, which was associated with the transboundary transport of pollutants before and during this period (Fig. 5c). The

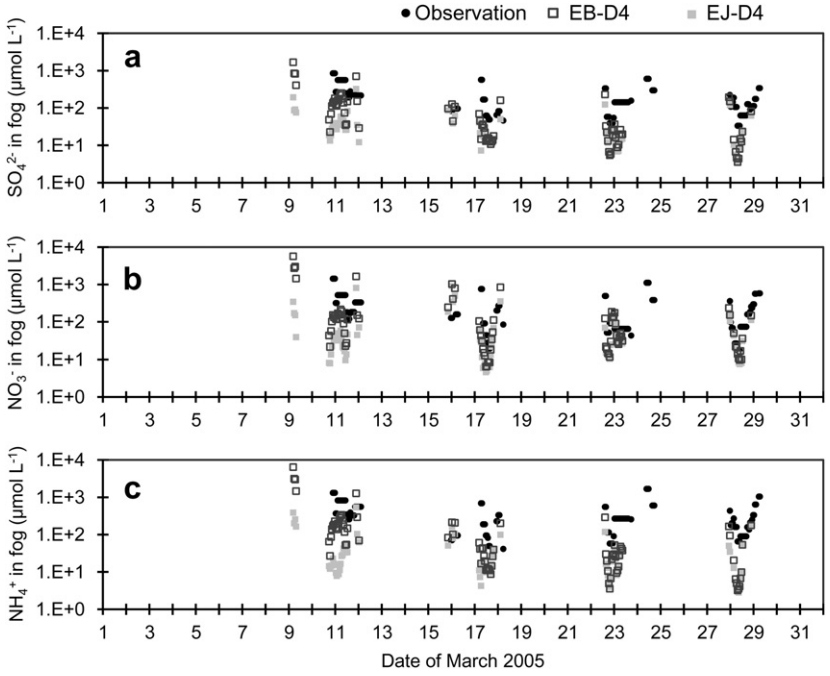

Fig. 6. Hourly time series of observed and model-predicted SO_4^{2-}, NO_3^- and NH_4^+ concentrations in fog water at the Mt. Rokko fog sampling site in March 2005.

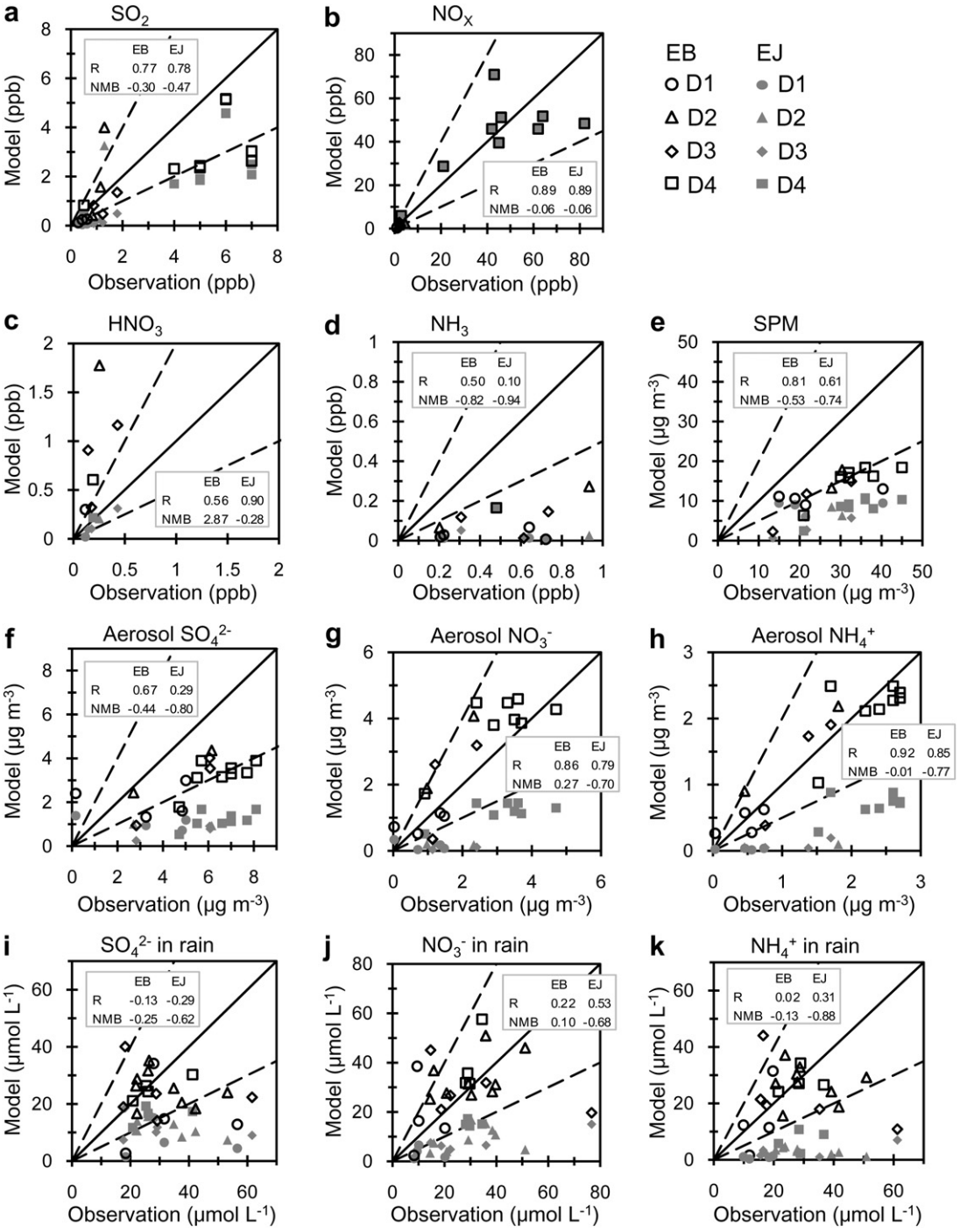

Fig. 7. Scatter plots of the observed versus model-predicted monthly mean concentrations of pollutants, with R and NMB in March 2005. Comparisons are shown for model predictions in the finest domains that contain the corresponding observation sites. 1:2 (dashed line) and 1:1 (solid line) reference lines are provided.

results indicate that ionic concentrations in fog water on Mt. Rokko are also affected by the transboundary air pollution.

4.3. Monthly mean concentrations and contributions of transboundary transport

Fig. 7 provides scatter plots of the observed versus model-predicted monthly mean concentrations, showing R and the normalized mean bias (NMB), which is defined as

$$\mathrm{NMB} = \frac{\overline{M}}{\overline{O}} - 1. \quad (6)$$

Dashed lines and solid line in each scatter plot in Fig. 7 are 1:2 and 1:1 reference lines, respectively. Fig. 8 shows spatial distributions of model-predicted monthly mean concentrations for EB, EB-D4 and EJ-D4. Table 3 summarizes monthly mean concentrations for EB-D4 and EJ-D4, and contribution rates of transboundary air pollution in D4. For most species, the model-predicted concentrations in EB

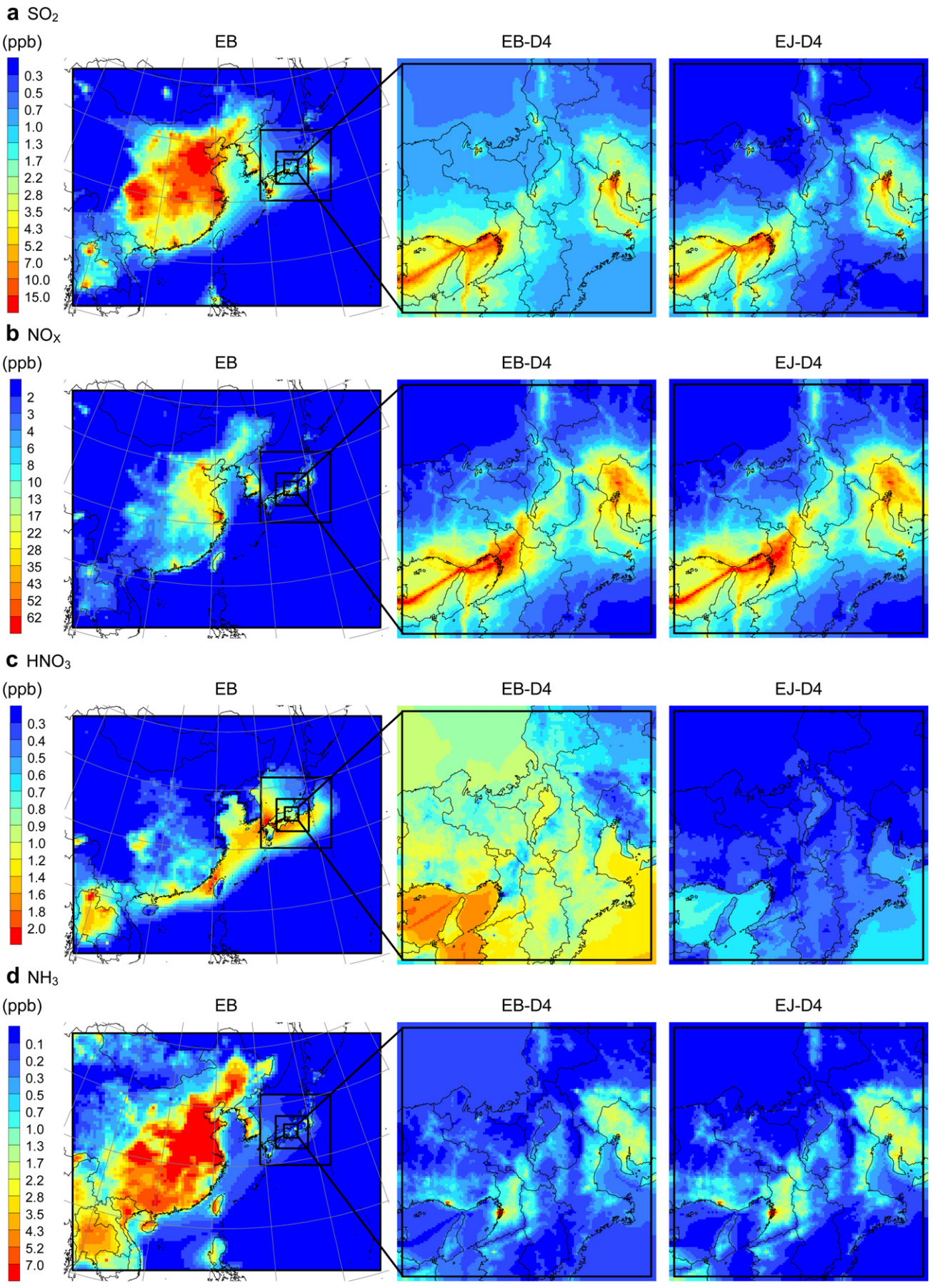

Fig. 8. Spatial distributions of model-predicted monthly mean concentrations of pollutants for EB, EB-D4 and EJ-D4 in March 2005. For ionic concentrations in fog, results are not shown in grid cells with fog frequencies below 1%, i.e. less than 8 h of fog duration in March 2005.

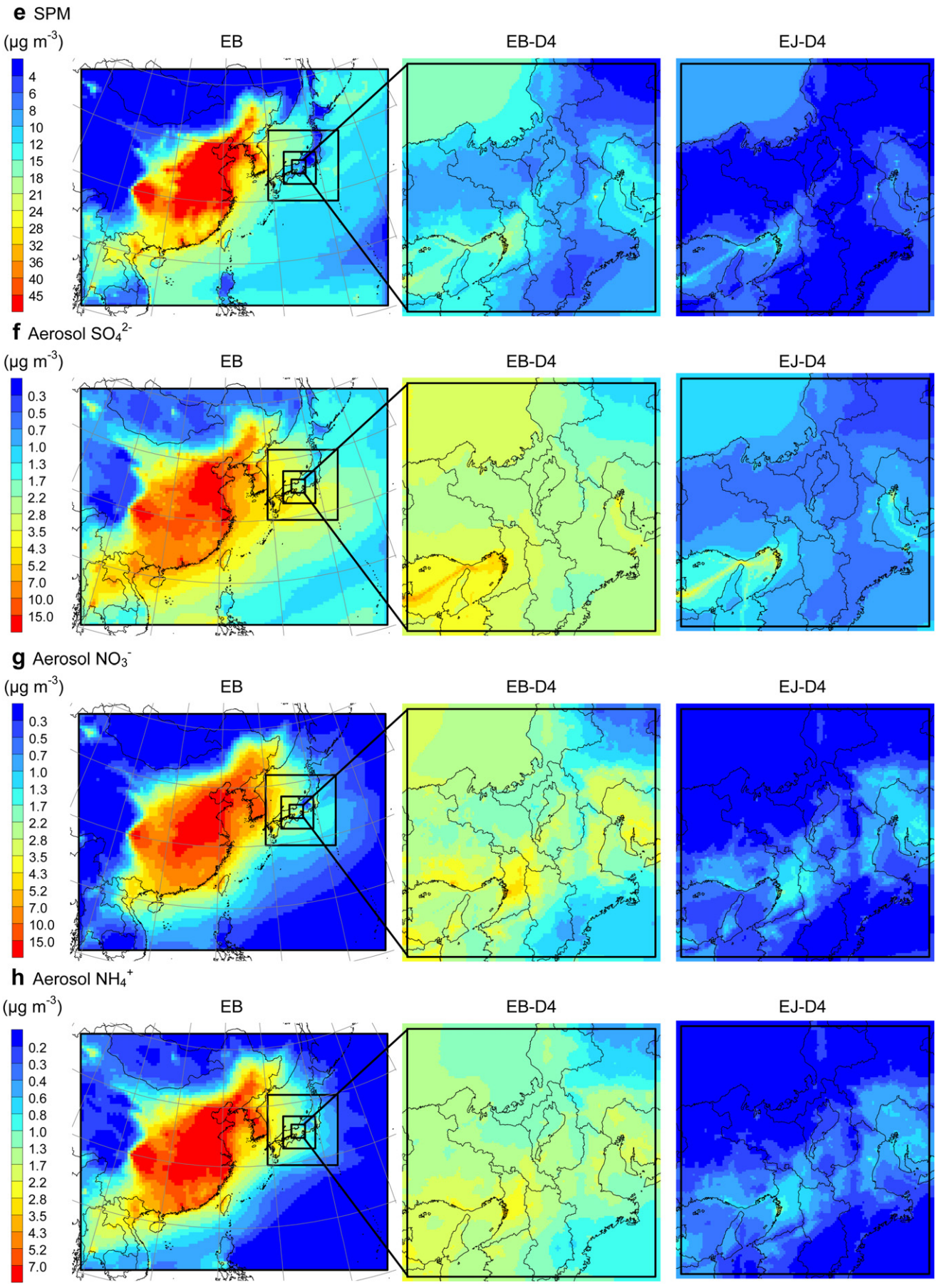

Fig. 8. (*continued*).

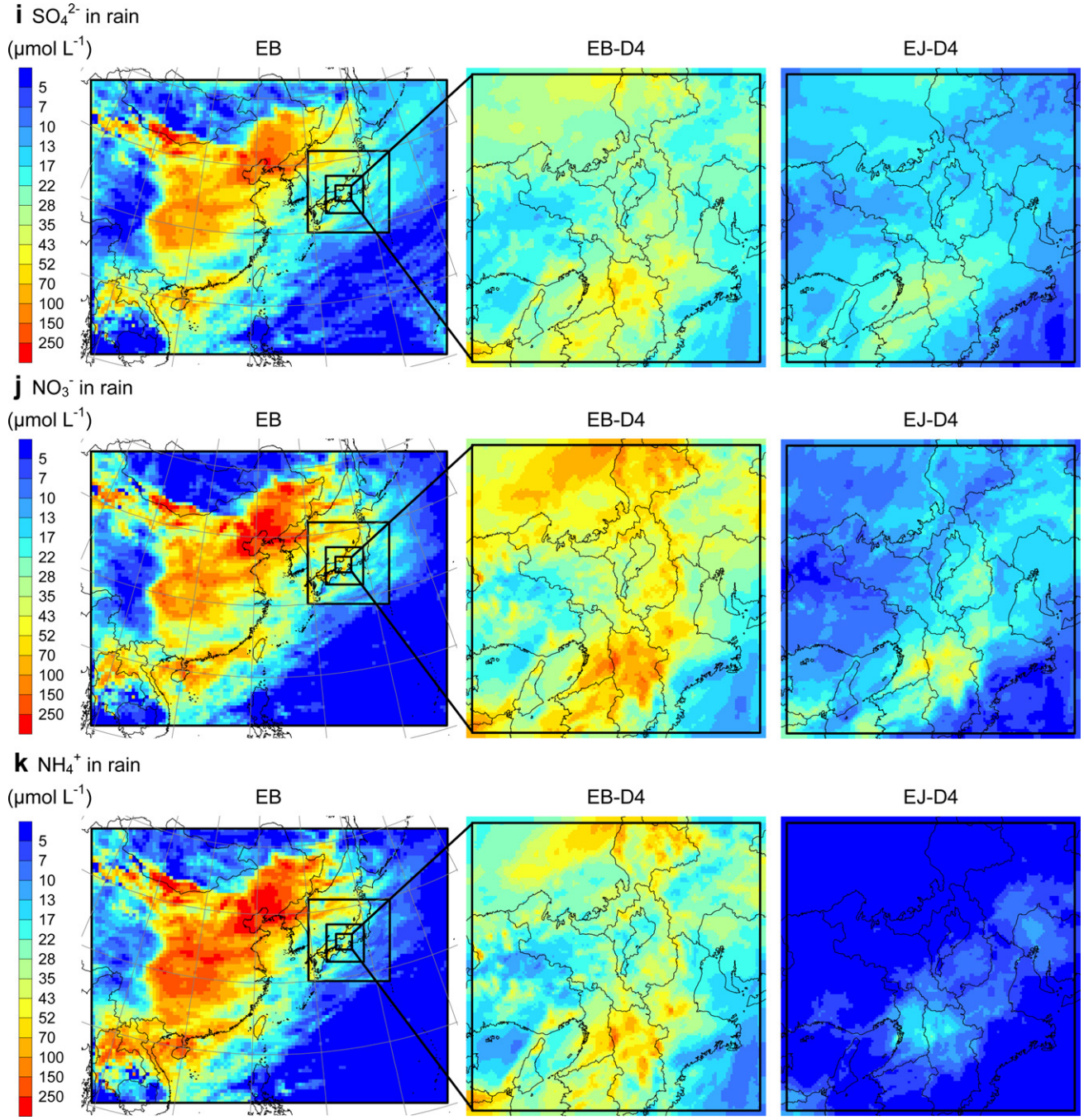

Fig. 8. (*continued*).

were higher and agreed better with the observations than those in EJ (Fig. 7), indicating that the model well simulated the transboundary air pollutions.

SO_2 was transported from the Asian Continent to Japan (Fig. 8a), but not as markedly as aerosol SO_4^{2-} (Fig. 8f). The contribution rates of the transboundary air pollution in D4 were 33% for SO_2 and 69% for aerosol SO_4^{2-}. Ichikawa et al. (1998) and Lin et al. (2008) estimated that the transboundary transport contributed approximately 40% of sulfur deposition in Japan for 1990, and 63% of anthropogenic sulfur deposition in Japan for 2001, respectively. Although direct comparison with these studies may not be appropriate as the current study focuses on pollutant concentrations in the Kinki Region of Japan for March 2005, the contribution rates of transboundary transport for concentrations of aerosol SO_4^{2-} (69%) and SO_4^{2-} in rain (47%) are reasonably consistent with the earlier data.

For NO_x, the spatial distributions in EB-D4 and EJ-D4 were almost consistent (Fig. 8b), with the contribution rate of the transboundary air pollution being 0%. The difference in the contributions of transboundary transport of SO_2 and NO_x in D4 may be attributed to the atmospheric lifetimes and the ratios of the local emissions to the total emissions in EB. While SO_2 emissions in D4 (18 mol s^{-1}) account for 0.1% of the total SO_2 emissions (19 016 mol s^{-1}), NO_x emissions in D4 (144 mol s^{-1}) account for 0.5% of the total NO_x emissions (29 831 mol s^{-1}).

The results of HNO_3 predictions in EB obviously overestimated the concentration levels (Fig. 7c). HNO_3 reacts with NH_3 to form

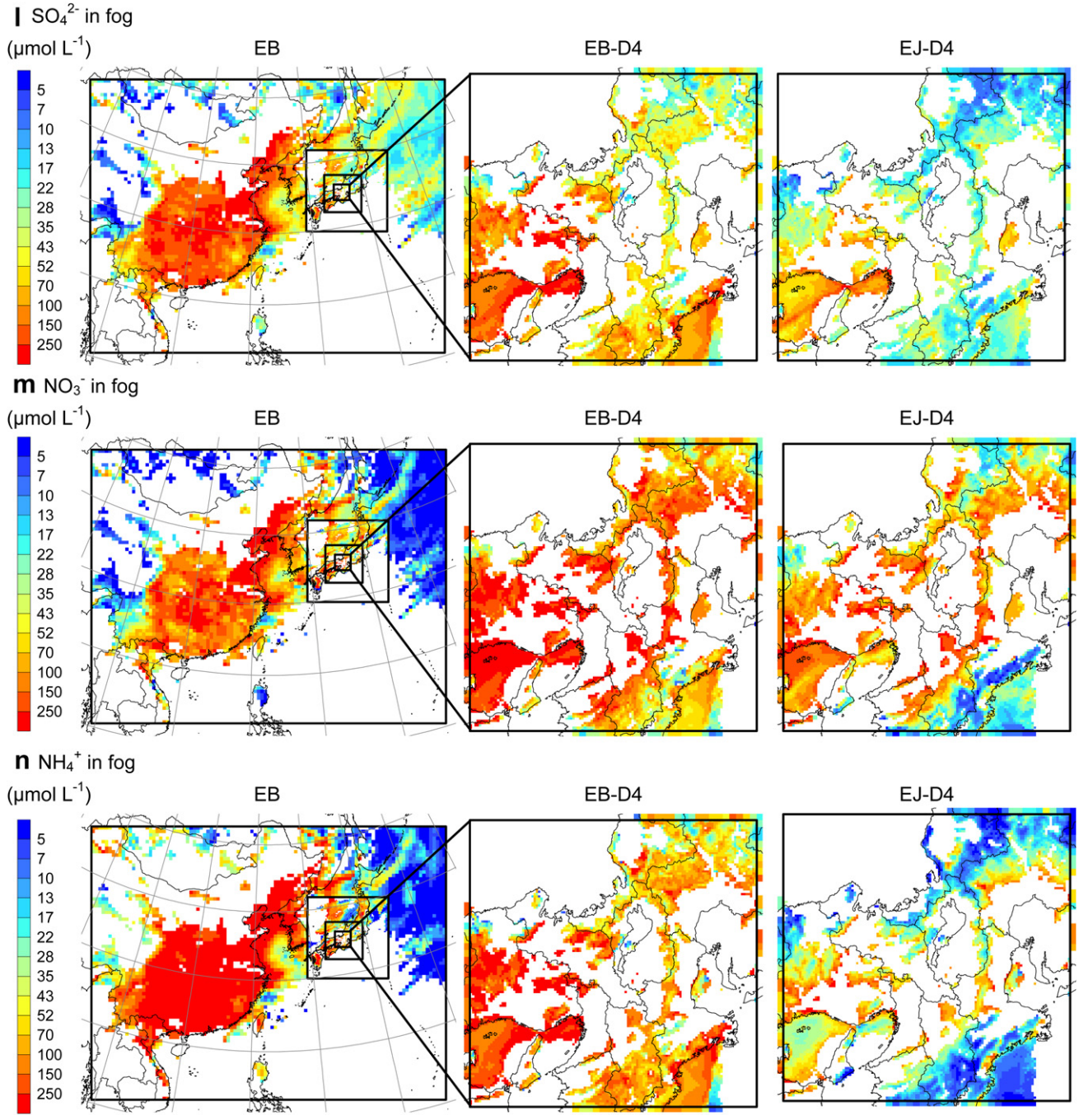

Fig. 8. (*continued*).

aerosol NH_4NO_3. The inverse spatial distribution patterns between HNO_3 and NH_3 indicate the direct reaction between them (Fig. 8c and d). In ocean areas with no NH_3 emission, HNO_3 was present in higher concentrations along the continental coast and transported to the Japan region, which caused the overestimations of HNO_3 in EB. The overestimation of HNO_3 was probably responsible for underestimation of NH_3 (Fig. 7d), and moderate overestimations of aerosol NO_3^- (Fig. 7g). Furthermore, the model probably underestimated the contribution rate of the transboundary air pollution for NH_3 (−1%) and overestimated the contribution rates for HNO_3 (62%), aerosol NO_3^- (82%). Chuang et al. (2008) reported that CMAQ version 4.4 with AERO3 might overestimate HNO_3 by not considering reactions between sea salt and HNO_3. Although the present study applied CMAQ version 4.7 with AERO5, which included sea salt emissions and the related reactions, the model still overestimated HNO_3 concentrations.

The discrepancies between the model predictions and observations in the current work may be also associated with uncertainties and inaccuracies in emission data and boundary conditions. For emission data, differences among emission inventories can be significant because of the large uncertainties in emission estimates. For example, the value of the total SO_2 emission for China in the 2006 Asia Emissions for INTEX-B (31.0 Tg $year^{-1}$), in which the SO_2 emission was estimated to increase by 36% during 2001–2006, still lower than the value in REAS for the year 2003 (36.6 Tg $year^{-1}$). Kannari et al. (2007) recognized that EAGrid2000-Japan included

Table 3
Monthly mean concentrations in EB-D4 and EJ-D4, and contribution rates of transboundary air pollution in D4 in March 2005.

	Mean concentration		Contribution of transboundary air pollution (%)
	EB-D4	EJ-D4	
SO_2 (ppb)	1.5	1.0	33
NO_x (ppb)	9.6	9.6	0
HNO_3 (ppb)	0.94	0.35	62
NH_3 (ppb)	0.29	0.29	−1
SPM ($\mu g\ m^{-3}$)	10.6	4.8	55
Aerosol SO_4^{2-} ($\mu g\ m^{-3}$)	2.73	0.86	69
Aerosol NO_3^- ($\mu g\ m^{-3}$)	2.23	0.41	82
Aerosol NH_4^+ ($\mu g\ m^{-3}$)	1.34	0.25	81
SO_4^{2-} in rain ($\mu mol\ L^{-1}$)	27	14	47
NO_3^- in rain ($\mu mol\ L^{-1}$)	43	13	71
NH_4^+ in rain ($\mu mol\ L^{-1}$)	30.3	3.9	87
SO_4^{2-} in fog ($\mu mol\ L^{-1}$)	75	28	62
NO_3^- in fog ($\mu mol\ L^{-1}$)	141	63	55
NH_4^+ in fog ($\mu mol\ L^{-1}$)	117	25	79

uncertainties within emission factors, particularly for NH_3 from agricultural sources. The uncertainty in NH_3 emission may be also responsible for the underestimation of NH_3. For boundary conditions of D1, the CMAQ default concentration profiles, which represent relatively clean air conditions, were used in the present work. However, Lin et al. (2008) used boundary conditions derived from global CTM and showed that the contribution of global inflows to sulfur deposition was significant over many parts of East Asia. Despite these uncertainties and inaccuracies, most model-predicted monthly mean values in EB were approximately within a factor of 2 (from −0.5 to 1.0 in terms of NMB) of the observations (Fig. 7).

For aerosols (Fig. 8e–h) and ionic concentrations in rain (Fig. 8i–k), the monthly mean values in EB-D4 were consistently higher than those in EJ-D4. The contribution rates of the transboundary air pollution in D4 ranged from 55 to 82% for aerosols and from 47 to 87% for ionic concentrations in rain. The spatial distribution patterns for SO_4^{2-}, NO_3^- and NH_4^+ concentrations in rain resembled one another as the concentrations were directly affected by the amount of precipitation. Similarly, the distribution patterns for the three ionic concentrations in fog (Fig. 8l–n) resembled one another as the concentrations were directly affected by LWC. The ionic concentrations in fog were generally higher and more spatially variable than those in rain, and were also strongly affected by the transboundary air pollution, with the contribution rates ranging from 55 to 79%. Fog is contaminated by ambient pollutants, but in the Kinki Region of Japan a considerable part of the air pollutants is transported from the Asian Continent. Consequently, ionic concentrations in fog as well as aerosol species and ionic concentrations in rain are strongly affected by the transboundary air pollution.

5. Conclusions

The MM5/CMAQ modeling system was employed to estimate the contribution of the transboundary transport to ionic concentrations in fog water in the Kinki Region of Japan for March 2005. The simulations were performed for EB with the total emissions and EJ with only the emissions from the Japan region, with the 4 nested modeling domains from D1 covering a wide area of East Asia to D4 covering most of the Kinki Region of Japan. For meteorological predictions, the statistical measures showed that the model simulated fairly well surface temperature and humidity in D2-D4 with GPV MSM, but not so accurately surface wind in D1 with NCEP FNL. Overall, the model well reproduced the meteorological fields in March 2005. At the fog sampling site on Mt. Rokko, the model generally captured the occurrence of fog, but tended to overestimate LWC. Although the model tended to overestimate the surface HNO_3 and aerosol NO_3^- concentrations, the model underestimated NO_3^- concentrations in fog as well as SO_4^{2-} and NH_4^+. The underestimations of ionic concentrations in fog occurred probably because of the overestimation of LWC. For most model predictions, the results for EB were in better agreement with the observations than those for EJ at the majority of observation sites. Most of monthly mean concentrations in EB were approximately within a factor of 2 of the observations, indicating that the model well simulated the long-range atmospheric transport from the Asian Continent to Japan despite some uncertainties and inaccuracies in emission data and boundary conditions. For aerosols and ionic concentrations in rain and fog, monthly mean concentrations in EB-D4 were consistently higher than those in EJ-D4. The contribution rates of the transboundary air pollution in D4 for SO_4^{2-}, NO_3^- and NH_4^+ were 69, 82 and 81% for aerosols, 47, 71 and 87% for ionic concentrations in rain, and 62, 55 and 79% for ionic concentrations in fog, respectively. The results of the current study show that the transboundary transported air pollutants strongly affects ionic concentrations in fog as well as aerosol species and ionic concentrations in rain in the Kinki Region of Japan.

Acknowledgements

We are grateful to the Hyogo and Osaka Prefectural Governments, JMA, and MOE of Japan for providing the observation data associated with this article. This work was partially supported by Grant-in-Aid for JSPS Fellows.

References

Aikawa, M., Hiraki, T., Shoga, M., Tamaki, M., 2005. Chemistry of fog water collected in the Mt. Rokko area (Kobe City, Japan) between April 1997 and March 2001. Water, Air, and Soil Pollution 160 (1–4), 373–393.
Aikawa, M., Hiraki, T., Tamaki, M., 2006. Comparative field study on precipitation, throughfall, stemflow, fog water, and atmospheric aerosol and gases at urban and rural sites in Japan. Science of the Total Environment 366 (1), 275–285.
Andres, R.J., Kasgnoc, A.D., 1998. A time-averaged inventory of subaerial volcanic sulfur emissions. Journal of Geophysical Research D: Atmospheres 103 (D19), 25251–25261.
Ballard, S.P., Golding, B.W., Smith, R.N.B., 1991. Mesoscale model experimental forecasts of the Haar of northeast Scotland. Monthly Weather Review 119, 2107–2123.
Baumgardner, R.E., Kronmiller, K.G., Anderson, J.B., Bowser, J.J., Edgerton, E.S., 2003. Estimates of cloud water deposition at mountain acid deposition program sites in the Appalachian mountains. Atmospheric Environment 33 (30), 5105–5114.
Brown, R., 1980. A numerical study of radiation fog with an explicit formulation of the microphysics. Quarterly Journal, Royal Meteorological Society 106 (450), 781–802.
Byun, D.W., Ching, J.K.S. (Eds.), 1999. Science Algorithms of the EPA Models-3 Community Multi-scale Air Quality (CMAQ) Modeling System. NERL, Research Triangle Park, NC.
Byun, D.W., Schere, K.L., 2006. Review of the governing equations, computational algorithms, and other components of the models-3 community multiscale air quality (CMAQ) modeling system. Applied Mechanics Reviews 59, 51–77.
Carmichael, G.R., Calori, G., Hayami, H., Uno, I., Cho, S.Y., Engardt, M., Kim, S.-B., Ichikawa, Y., Ikeda, Y., Woo, J.-H., Ueda, H., Amann, M., 2002. The MICS-Asia study: model intercomparison of long-range transport and sulfur deposition in East Asia. Atmospheric Environment 36 (2), 175–199.
Carmichael, G.R., Sakurai, T., Streets, D., Hozumi, Y., Ueda, H., Park, S.U., Fung, C., Han, Z., Kajino, M., Engardt, M., Bennet, C., Hayami, H., Sartelet, K., Holloway, T., Wang, Z., Kannari, A., Fu, J., Matsuda, K., Thongboonchoo, N., Amann, M., 2008. MICS-Asia II: the model intercomparison study for Asia Phase II methodology and overview of findings. Atmospheric Environment 42 (15), 3468–3490.
Carter, W.P.L., 2000. Documentation of the SAPRC-99 Chemical Mechanism for VOC Reactivity Assessment. Final Report to California Air Resources Board Contract No. 92-329, and (in part) 95–308.
Chen, F., Dudhia, J., 2001. Coupling an advanced land-surface/hydrology model with the Penn State/NCAR MM5 modeling system — Part I: model implementation and sensitivity. Monthly Weather Review 129 (4), 569–585.
Chuang, M.-T., Fu, J.S., Jang, C.J., Chan, C.-C., Ni, P.-C., Lee, C.-Te, 2008. Simulation of long-range transport aerosols from the Asian Continent to Taiwan by a Southward Asian high-pressure system. Science of the Total Environment 406 (1–2), 168–179.
Dawson, T.E., 1998. Fog in the California redwood forest: ecosystem inputs and use by plants. Oecologia 117 (4), 476–485.
Dudhia, J., 1989. Numerical study of convection observed during the winter monsoon experiment using a mesoscale two-dimensional model. Journal of the Atmospheric Sciences 46 (20), 3077–3107.

Emery, C., Tai, E., Yarwood, G., 2001. Enhanced Meteorological Modeling and Performance Evaluation for Two Texas Ozone Episodes. Project Report prepared for the Texas Natural Resource Conservation Commission.

Eugster, W., Burkard, R., Holwerda, F., Scatena, F.N., Bruijnzeel, L.A.S., 2006. Characteristics of fog and fogwater fluxes in a Puerto Rican elfin cloud forest. Agricultural and Forest Meteorology 139 (3–4), 288–306.

Fu, G., Guo, J., Xie, S.-P., Duan, Y., Zhang, M., 2006. Analysis and high-resolution modeling of a dense sea fog event over the Yellow Sea. Atmospheric Research 81 (4), 293–303.

Gong, S.L., 2003. A parameterization of sea-salt aerosol source function for sub- and super-micron particles. Global Biogeochemical Cycles 17 (4), 8/1–8/7.

Grell, G.A., Dudhia, J., Stauffer, D.R., 1994. A Description of the Fifth-generation Penn State/NCAR Mesoscale Model (MM5). NCAR Technical Note NCAR/TN-398 + STR, pp.117.

Hong, S.Y., Pan, H.L., 1996. Nonlocal boundary layer vertical diffusion in a medium-range forecast model. Monthly Weather Review 124, 2322–2339.

Ichikawa, Y., Hayami, H., Fujita, S., 1998. A long-range transport model for East Asia to estimate sulfur deposition in Japan. Journal of Applied Meteorology 37 (10 Part II), 1364–1374.

Igawa, M., Tsutsumi, Y., Mori, T., Okochi, H., 1998. Fogwater chemistry at a mountainside forest and the estimation of the air pollutant deposition via fog droplets based on the atmospheric quality at the mountain base. Environmental Science and Technology 32 (11), 1566–1572.

Kannari, A., Tonooka, Y., Baba, T., Murano, K., 2007. Development of multiple-species 1 km × 1 km resolution hourly basis emissions inventory for Japan. Atmospheric Environment 41 (16), 3428–3439.

Kobayashi, T., Nakagawa, Y., Tamaki, M., Hiraki, T., Aikawa, M., 2001. Cloud water deposition to forest canopies of Cryptomeria japonica at Mt. Rokko, Kobe, Japan. Water, Air, and Soil Pollution 130 (1–4 II), 601–606.

Lee, S.-H., Kim, Y.-K., Kim, H.-S., Lee, H.-W., 2007. Influence of dense surface meteorological data assimilation on the prediction accuracy of ozone pollution in the southeastern coastal area of the Korean Peninsula. Atmospheric Environment 41 (21), 4451–4465.

Lin, M., Oki, T., Bengtsson, M., Kanae, S., Holloway, T., Streets, D.G., 2008. Long-range transport of acidifying substances in East Asia-Part II. Source–receptor relationships. Atmospheric Environment 42 (24), 5956–5967.

Murano, K., 2006. International Co-operative Survey to Clarify the Trans-boundary Air Pollution Across the Northern Hemisphere (Abstract of the Final Report). Summary Report of Research Results under the GERF (Global Environment Research Fund) in FY2004, pp. 237–243, Research and Information Office, Global Environment Bureau, Ministry of the Environment, Government of Japan.

Musson-Genon, L., 1987. Numerical simulation of a fog event with a one-dimensional boundary layer model. Monthly Weather Review 115 (2), 592–607.

Neal, C., Reynolds, B., Neal, M., Hill, L., Wickham, H., Pugh, B., 2003. Nitrogen in rainfall, cloud water, throughfall, stemflow, stream water and groundwater for the Plynlimon catchments of mid-Wales. Science of the Total Environment 314-316, 121–151.

Ohara, T., Akimoto, H., Kurokawa, J., Horii, N., Yamaji, K., Yan, X., Hayasaka, T., 2007. An Asian emission inventory of anthropogenic emission sources for the period 1980–2020. Atmospheric Chemistry and Physics 7 (16), 4419–4444.

Pagowski, M., Gultepe, I., King, P., 2004. Analysis and modeling of an extremely dense fog event in southern Ontario. Journal of Applied Meteorology 43 (1), 3–16.

Pielke, R.A., Cotton, W.R., Walko, R.L., Tremback, C.J., Lyons, W.A., Grasso, L.D., Nicholls, M.E., Moran, M.D., Wesley, D.A., Lee, T.J., Copeland, J.H., 1992. A comprehensive meteorological modeling system—RAMS. Meteorology and Atmospheric Physics 49, 69–91.

Richter, A., Burrows, J.P., Nüß, H., Granier, C., Niemeier, U., 2005. Increase in tropospheric nitrogen dioxide over China observed from space. Nature 437 (7055), 129–132.

Seto, S., Nakamura, A., Noguchi, I., Ohizumi, T., Fukuzaki, N., Toyama, S., Maeda, M., Hayashi, K., Hara, H., 2002. Annual and seasonal trends in chemical composition of precipitation in Japan during 1989–1998. Atmospheric Environment 36 (21), 3505–3517.

Shimadera, H., Shrestha, K.L., Kondo, A., Kaga, A., Inoue, Y., 2008. Fog simulation using a mesoscale model in and around the Yodo River Basin, Japan. Journal of Environmental Sciences 20 (7), 838–845.

Sokhi, R.S., San Joseć, R., Kitwiroon, N., Fragkou, E., Pećrez, J.L., Middleton, D.R., 2006. Prediction of ozone levels in London using the MM5-CMAQ modelling system. Environmental Modelling and Software 21 (4), 566–576.

Stoelinga, M.T., Warner, T.T., 1999. Nonhydrostatic, mesobeta-scale model simulations of cloud ceiling and visibility for an East Coast winter precipitation event. Journal of Applied Meteorology 38 (4), 385–404.

Streets, D.G., Yarber, K.F., Woo, J.-H., Carmichael, G.R., 2003. Biomass burning in Asia: annual and seasonal estimates and atmospheric emissions. Global Biogeochemical Cycles 17 (4), 10/1–10/20.

Tamamura, S., Sato, T., Ota, Y., Wang, X., Tang, N., Hayakawa, K., 2007. Long-range transport of polycyclic aromatic hydrocarbons (PAHs) from the eastern Asian continent to Kanazawa, Japan with Asian dust. Atmospheric Environment 41 (12), 2580–2593.

Tesche, T.W., Morris, R., Tonnesen, G., McNally, D., Boylan, J., Brewer, P., 2006. CMAQ/CAMx annual 2002 performance evaluation over the eastern US. Atmospheric Environment 40 (26), 4906–4919.

Vong, R.J., Sigmon, J.T., Mueller, S.F., 1991. Cloud water deposition to Appalachian forests. Environmental Science and Technology 25 (6), 1014–1021.

Wu, S.-Y., Krishnan, S., Zhang, Y., Aneja, V., 2008. Modeling atmospheric transport and fate of ammonia in North Carolina-Part I: evaluation of meteorological and chemical predictions. Atmospheric Environment 42 (14), 3419–3436.

Zdunkowski, W.G., Nielsen, B.C., 1969. A preliminary prediction analysis of radiation fog. Pure and Applied Geophysics (PAGEOPH) 75 (1), 278–299.

Zhang, K.M., Knipping, E.M., Wexler, A.S., Bhave, P.V., Tonnesen, G.S., 2005. Size distribution of sea-salt emissions as a function of relative humidity. Atmospheric Environment 39 (18), 3373–3379.

Zhang, M., Uno, I., Zhang, R., Han, Z., Wang, Z., Pu, Y., 2006. Evaluation of the models-3 community multi-scale air quality (CMAQ) modeling system with observations obtained during the TRACE-P experiment: comparison of ozone and its related species. Atmospheric Environment 40 (26), 4874–4882.

Zhang, Q., Streets, D.G., Carmichael, G.R., He, K., Huo, H., Kannari, A., Klimont, Z., Park, I., Reddy, S., Fu, J.S., Chen, D., Duan, L., Lei, Y., Wang, L., Yao, Z., 2009. Asian emissions in 2006 for the NASA INTEX-B mission. Atmospheric Chemistry and Physics Discussions 9 (1), 4081–4139.